Atmospheric Environment 117 (2015) 200–211

Contents lists available at ScienceDirect

Atmospheric Environment

journal homepage: www.elsevier.com/locate/atmosenv

Primary emissions and secondary organic aerosol formation from the exhaust of a flex-fuel (ethanol) vehicle

R. Suarez-Bertoa [a, *], A.A. Zardini [a], S.M. Platt [b], S. Hellebust [c], S.M. Pieber [b], I. El Haddad [b], B. Temime-Roussel [c], U. Baltensperger [b], N. Marchand [c], A.S.H. Prévôt [b], C. Astorga [a, **]

[a] European Commission, Joint Research Centre (JRC), Institute for Energy and Transport (IET), Sustainable Transport Unit, 21027 Ispra, VA, Italy
[b] Laboratory of Atmospheric Chemistry, Paul Scherrer Institute (PSI), Villigen 5232, Switzerland
[c] Aix-Marseille Université, CNRS, LCE FRE 3416, 13331 Marseille, France

HIGHLIGHTS

- Emissions from a flex-fuel vehicle, fueled with E85 and E75, lead to SOA formation.
- These vehicles show higher regulated and unregulated emissions at −7 °C.
- Unregulated emissions are mainly composed of ethanol and acetaldehyde.
- SOA may arise from oxygenated compounds present in the exhaust.

ARTICLE INFO

Article history:
Received 12 January 2015
Received in revised form
11 June 2015
Accepted 8 July 2015
Available online 15 July 2015

Keywords:
Ozone formation potential
Secondary organic aerosol
Acetaldehyde
Carbonyls
Unregulated emissions
Aerosol mass spectrometry

ABSTRACT

Incentives to use biofuels may result in increasing vehicular emissions of compounds detrimental to air quality. Therefore, regulated and unregulated emissions from a Euro 5a flex-fuel vehicle, tested using E85 and E75 blends (gasoline containing 85% and 75% of ethanol (vol/vol), respectively), were investigated at 22 and −7 °C over the New European Driving Cycle, at the Vehicle Emission Laboratory at the European Commission Joint Research Centre Ispra, Italy. Vehicle exhaust was comprehensively analyzed at the tailpipe and in a dilution tunnel. A fraction of the exhaust was injected into a mobile smog chamber to study the photochemical aging of the mixture. We found that emissions from a flex-fuel vehicle, fueled by E85 and E75, led to secondary organic aerosol (SOA) formation, despite the low aromatic content of these fuel blends. Emissions of regulated and unregulated compounds, as well as emissions of black carbon (BC) and primary organic aerosol (POA) and SOA formation were higher at −7 °C. The flex-fuel unregulated emissions, mainly composed of ethanol and acetaldehyde, resulted in very high ozone formation potential and SOA, especially at low temperature (860 mg O_3 km^{-1} and up to 38 mg C kg^{-1}). After an OH exposure of 10×10^6 cm^{-3} h, SOA mass was, on average, 3 times larger than total primary particle mass emissions (BC + POA) with a high O:C ratio (up to 0.7 and 0.5 at 22 and −7 °C, respectively) typical of highly oxidized mixtures. Furthermore, high resolution organic mass spectra showed high 44/43 ratios (ratio of the ions m/z 44 and m/z 43) characteristic of low-volatility oxygenated organic aerosol. We also hypothesize that SOA formation from vehicular emissions could be due to oxidation products of ethanol and acetaldehyde, both short-chain oxygenated VOCs, e.g. methylglyoxal and acetic acid, and not only from aromatic compounds.

© 2015 The Authors. Published by Elsevier Ltd. This is an open access article under the CC BY-NC-ND license (http://creativecommons.org/licenses/by-nc-nd/4.0/).

1. Introduction

The use of biofuels is increasing worldwide as a result of a promotion to meet the growing demand of transport related energy as well as to reduce greenhouse gas (GHG) emissions (European Commission, 2009). Biofuels were seen as a measure to reduce emissions of GHGs from road transport because they were

* Corresponding author.
** Corresponding author.
E-mail addresses: ricardo.suarez-bertoa@jrc.ec.europa.eu (R. Suarez-Bertoa), covadonga.astorga-llorens@jrc.ec.europa.eu (C. Astorga).

http://dx.doi.org/10.1016/j.atmosenv.2015.07.006
1352-2310/© 2015 The Authors. Published by Elsevier Ltd. This is an open access article under the CC BY-NC-ND license (http://creativecommons.org/licenses/by-nc-nd/4.0/).

considered CO_2 neutral. The EU has set a target of 10% share of renewable energy in the transport sector, to be complied with by 2020 (2009/28/EC). Biofuels covered 4.3% of this share in 2010 (80% biodiesel, 20% ethanol) (European Commission, 2013).

Previous studies have suggested that increasing ethanol content in fuel blends reduces the emission of some regulated gases (CO and total hydrocarbons, THC) and CO_2 (Clairotte et al., 2013; Durbin et al., 2007; Graham et al., 2008; Andrade et al., 1998). However, despite promising benefits in terms of reducing regulated compounds and CO_2 emissions, it has been shown that higher ethanol concentrations in fuel blends lead to higher emissions of ethanol and carbonyl compounds, mainly acetaldehyde, which are associated with urban air pollution and the formation of persistent pollutants (Clairotte et al., 2013; Durbin et al., 2007; Graham et al., 2008; Andrade et al., 1998). In the atmosphere, ethanol is a precursor of acetaldehyde and peroxyacetyl nitrate (PAN); hence, a change in the ethanol emissions will affect atmospheric composition and chemistry. Photochemical oxidation by OH radicals is the main atmospheric sink of ethanol (Atkinson et al., 2006). Ethanol's atmospheric life time is about 4 days (Atkinson et al., 2006), with acetaldehyde being the main oxidation product at ~95% yield. Acetaldehyde is classified as a hazardous air pollutant by the U.S. EPA (Chemical Summary for Acetaldehyde), and its subsequent oxidation can also lead to production of ozone (O_3) and PAN. Thus, the fate of atmospheric reactive nitrogen (NOy) could be affected by an increase in the PAN to NOy ratio (Millet et al., 2012a). Moreover, modeling studies have reported that in the case of a considerable shift from gasoline to ethanol blends, urban ozone levels would increase (Cook et al., 2011; Diana and Mark, 2012; Jacobson, 2007).

Previous studies have shown that, while in some metropolitan areas formaldehyde is almost always the predominant carbonyl emitted by vehicles (acetaldehyde/formaldehyde ratio emitted <1), for Brazilian cities acetaldehyde/formaldehyde ratios are $\geq$1 (Corrêa et al., 2003; Nguyen et al., 2001; Corrêa et al., 2010). This behavior has been attributed to the use of ethanol and gasohol (gasoline with 24% of ethanol content) as fuels (Corrêa et al., 2003; Nguyen et al., 2001; Corrêa et al., 2010). Incomplete combustion of ethanol results in higher acetaldehyde emission compared to formaldehyde. Carbonyl compounds are among the main volatile organic compounds (VOCs) present in the atmosphere of cities where ethanol blended fuels are used (Corrêa et al., 2010). They are also the main ozone precursors in those cities (Corrêa et al., 2010).

Atmospheric reactions of VOCs have been of great interest for the study of secondary organic aerosol (SOA) formation. SOA is a major contributor to airborne particulate matter (Hallquist et al., 2009), which is associated with adverse health effects (Pope et al., 2002). SOA not only impoverishes air quality but also has an impact on climate via scattering and, absorption of light as well as aerosol–cloud interactions (Ramaswamy et al., 2007; Orlando et al., 1999; Saleh et al., 2014).

It has been shown that atmospheric photooxidation of several VOCs generates large amounts of highly oxidized compounds, such as multifunctional carbonyl compounds (Jang and Kamens, 2001), which are major SOA components. Many of these oxidized VOCs have lower vapor pressure and condense to produce SOA. However, another pathway leading to SOA production may involve non-radical reactions e.g. hydration, polymerization, hemiacetal and acetal formation, or aldol condensation (Jang et al., 2002; Kroll and Seinfeld, 2008). These reactions are influenced by the relationship between media acidity and relative humidity (RH). The key compounds in these reactions are atmospheric carbonyls and alcohols, such as those found in the exhaust of ethanol-fueled vehicles, and water and inorganic acids that act as catalysts. The main atmospheric inorganic acids that could act as catalysts are sulfuric acid (H_2SO_4) and nitric acid (HNO_3), produced via oxidation of SO_2 and NOx (Jang et al., 2002; Pitts and Finlayson-Pitts, 2000).

Jang et al. (2002) proposed condensation and polymerization reactions of carbonyls as a possible explanation of SOA mass increase; Kalberer et al. (2006) showed that non-radical compounds induced acetal polymerization with methylglyoxal being the main monomeric unit. The polymers formed constituted a large fraction of SOA produced. They also suggested that other non-radical reactions such as aldol condensation reaction could occur in the complex organic mixture of the aerosol. Therefore, the study of new emission sources of alcohols and carbonyls is of major importance since they could lead to a substantial change in urban atmospheric chemistry.

Here we present results from a comprehensive study of the exhaust emissions of a Euro 5a compliant flex-fuel vehicle over the New European Driving Cycle (NEDC) at 22 and −7 °C carried out in the Vehicle Emission Laboratory (VELA) at the European Commission Joint Research Centre Ispra, Italy. Primary emissions, and for the first time secondary organic aerosol formation from aging of diluted exhaust from a flex-fuel vehicle fueled using E85 and E75 blends at 22 and −7 °C are reported.

2. Experimental section

The present study was conducted in the Vehicle Emission Laboratory (VELA) at the European Commission Joint Research Centre Ispra, Italy using a certified chassis dynamometer climatic cell combined with a mobile smog chamber (Laboratory of Atmospheric Chemistry, Paul Scherrer Institute, Switzerland) for gas/particle analysis during photochemical aging (see Fig. 1 for test cell configuration and Platt et al. (2013) for details on the smog chamber).

The VELA facility comprises a climatic test cell with controlled temperature and RH to simulate a variety of ambient conditions (temperature range: −10 to 35 °C; RH range: 50–80 %). Tests were performed on a chassis dynamometer (inertia range: 454–4500 kg), designed for two and four-wheel drive light duty vehicles (LDVs) (two 1.22 m roller benches – MAHA GmbH, Germany). The emissions were fed to a Constant Volume Sampler (CVS, Horiba, Japan) using a critical Venturi nozzle to regulate the flow (CVS flow range: 3–30 m^3 min^{-1}). A series of thermocouples monitored the temperature of the oil, cooling water, exhaust, and ambient conditions. A universal exhaust gas oxygen (UEGO) type sensor was connected to the tailpipe to follow the air to fuel ratio.

A flex-fuel light duty vehicle (hereinafter FFV) was tested (see technical details in Table 1) over the New European Driving Cycle (NEDC). The vehicle complied with Euro 5a spark ignition EU emission standards ((EC) No 692/2008) (European Commission, 2008). The NEDC is a cold-start driving cycle (i.e., performed with a cold engine at the beginning of the test cycle). It includes a first urban phase of 780 s (UDC) followed by an extra-urban phase of 400 s (EUDC). The tests were conducted at test cell temperature of 22 and −7 °C, and at 50 ± 2% RH. The temperature refers not only to the cell temperature but also to the vehicle's oil temperature at the beginning of each test (±1 °C). The vehicle was kept inside the climatic cell under the NEDC typical conditions (known as the soaking time) for at least 12 h. The vehicle was fueled with summer E85 and winter E75 blends (85 and 75% vol/vol ethanol content, respectively) when tested at 22 and −7 °C, respectively. A detailed description of the fuels' characteristics is available in Table 2.

Exhaust emissions were sampled online at the vehicle tailpipe, offline after dilution (integrated offline measurements, as required by the legislation) (The Council of the European Communities, 1970), and a constant fraction of the exhaust was injected during the whole driving cycle into the smog chamber for subsequent simulation of photochemical aging (Fig. 1). Instruments and

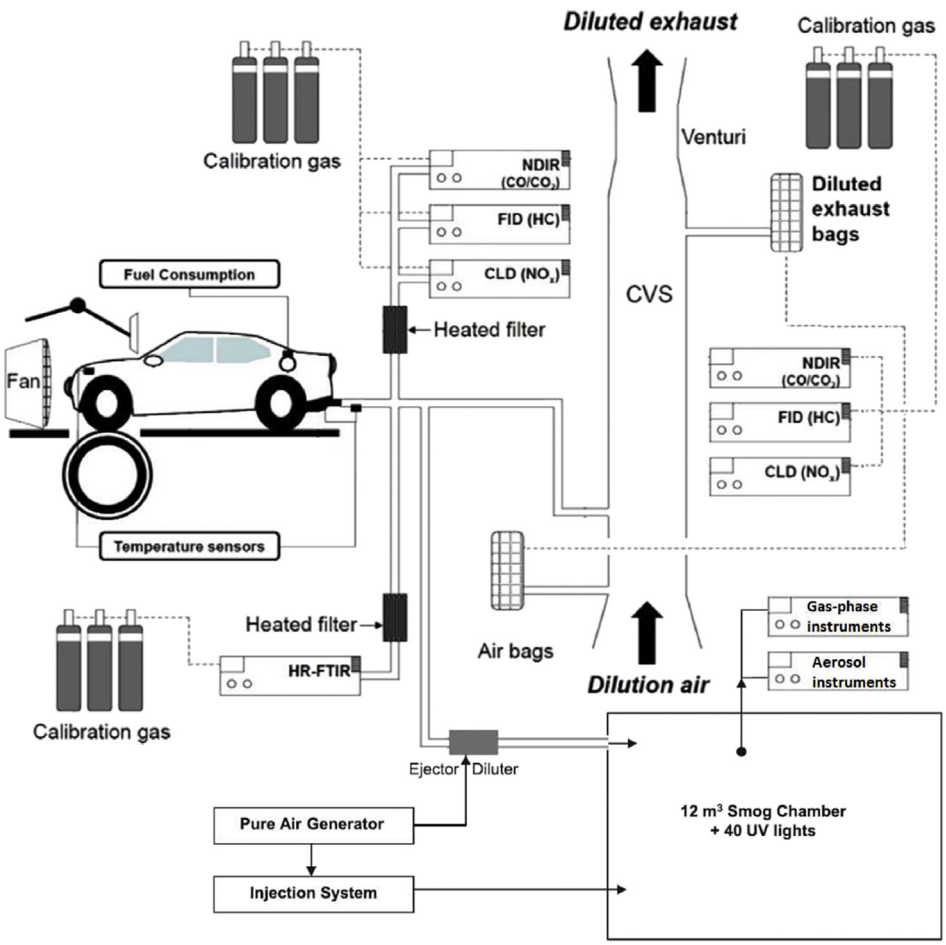

Fig. 1. Schematic of the experimental setup.

Table 1
Vehicle specifications.

Features	FFV
Combustion type	Spark ignition
Year of registration	2012
EU emission standard	Euro 5a
After-treatment	Three-way catalyst
Fuel system	Direct injection
Engine power (kW)	132
Engine displacement (cm^3)	1596
Odometer (km)	24,334

Table 2
Fuel specifications.

Parameter	Method	Unit	E75	E85
RON[a]	ISO 5164	–	102.9	107.8
MON[b]	ISO 5163	–	88.4	89.0
Density at 15 °C	ASTM D 4052	kg m^{-3}	772.8	785.7
DVPE[c] at 100F	EN 13016-1	kPa	50.1	35.1
GCV[d]	ASTM D 3338	MJ kg^{-1}	30.85	29.43
Sulfur (S)	ASTM D 5453	mg kg^{-1}	<3	3.2
Carbon (C)	ASTM D 3343	mass %	60.4	57.4
Hydrogen (H)	ASTM D 3343	mass %	13.1	13.1
Nitrogen (N)	ASTM D 9291	mass %	<0.75	<0.75
Oxygen (O)	EN 13132	mass %	26.5	29.5

[a] Research Octane Number.
[b] Motor Octane Number.
[c] Dry Vapor Pressure Equivalent.
[d] Gross Calorific Value.

methods deployed to characterize primary emissions and SOA formation in the smog chamber are summarized in Platt et al. (2013).

2.1. CVS and tailpipe analytical instrumentation

The vehicle's regulated emissions were measured in conformity with directive 70/220/EEC and its following amendments, with an integrated setup (MEXA-7400HTR-LE, HORIBA) that analyzed diluted gas from the CVS. Gaseous emissions were analyzed from a set of Tedlar bags. The bags were filled with diluted exhaust from the CVS (Automatic Bag Sampler, CGM electronics) and CO, total hydrocarbons (THC), NOx, and CO_2 concentrations were measured using the following techniques: non-dispersive infrared (for CO/CO_2), a chemiluminescence (for NOx) and a heated (191 °C) flame ionization detector (FID; for THC). Gaseous compounds contained in the raw exhaust were monitored at 1 Hz acquisition frequency by a High Resolution Fourier Transform Infrared spectrometer (FTIR – MKS Multigas analyzer 2030-HS, Wilmington, MA, USA). The method is described in more detail in the literature (Clairotte et al., 2012), therefore, only a brief description is given here. The device consists of a silicon carbide source (at 1200 °C), a multipath cell (optical length: 5.11 m), a Michelson interferometer (spectral resolution: 0.5 cm^{-1}, spectral range: 600–3500 cm^{-1}) and a liquid nitrogen cooled mercury cadmium telluride detector (MCT).

The raw exhaust was sampled directly from the tailpipe of the vehicle with a heated PTFE (polytetrafluoroethylene) line and a

pumping system (flow: ca. 10 L min^{-1}, *T*: 191 °C) in order to avoid condensation and/or adsorption of hydrophilic compounds (e.g., ethanol, ammonia). The residence time of the undiluted exhaust gas in the heated line before the FTIR measurement cell was less than 2 s. The ambient pressure during the measurement was 1013 hPa (±20), and the temperature of the gas cell of the FTIR was set to 191 °C. Another set of analyzers, i.e., non-dispersive infrared (for CO/CO_2) and chemiluminescence detector (for NOx) were also connected to the tailpipe allowing a time-resolved (at 1 Hz) measurement of these compounds from the raw exhaust. CO, CO_2 and NOx measurements from the previously described analyzers were used to synchronize the FTIR signal. Regulated and unregulated emission profiles showed very good repeatability (see Figs. 2 and 3 and Fig. S1). An example of the repeatability achieved for CO_2 emission profiles, oil temperature and exhaust temperature can be seen in Fig. S1 of the supplementary material.

The raw exhaust flow was determined by subtracting the flow of dilution air introduced into the tunnel, measured with a Venturi system, to the total flow of the dilution tunnel, measured by a sonic Venturi (Horiba). Mass flows were derived from the exhaust gas flow rates (m^3 s^{-1}) and from the measured concentration (ppmv). Emission factors (mg km^{-1}) were calculated from the integrated mass flow and the total driving distance of the NEDC (11 km).

Previous studies pointed out a poor sensitivity of the FID towards oxygenated VOCs emitted in the exhaust from engines fueled with high ethanol blended mixtures (Wallner, 2011; Erlandsson et al., 2010). Therefore, the time-resolved THC volumetric concentrations measured with the FID were corrected using the concentrations measured with the FTIR of ethanol, methanol, formaldehyde and acetaldehyde, as described by Clairotte et al. (2013).

The European Air Quality Directive on Ozone, 2002/3/EC (The European Parliament and The Council of the European Union, 2002) requires the analysis of 30 VOCs, including 29 C_2–C_9 hydrocarbons and formaldehyde, since they are considered, together with nitrogen oxides, the main ozone precursors in urban air. Most of these compounds were not present in the FFV's exhaust; therefore, a selection of compounds that are considered ozone precursors: carbonyl compounds, ethanol, carbon monoxide and C_2 hydrocarbons (ethane, ethylene and acetylene), were monitored at the vehicle tailpipe with the FTIR in order to estimate the ozone formation potential (OFP) of the emissions. The OFPs of these compounds were calculated in accordance to the maximum incremental reactivity concept (MIR) (Carter, 1994). The MIR concept is based on a scenario where optimum conditions of precursor/NOx ratios yield maximum ozone formation. The OFP is presented as the sum of the ozone produced from each precursor emitted over the whole cycle.

2.2. Smog chamber and integrated instrumentation

The smog chamber was located inside the vehicle test cell and thus operated at the same temperature. Instruments were located outside the test cell and operated at room temperature. Smog chamber temperature is measured at 3 locations: at the top and the bottom of the chamber and in the gas phase sampling line downstream the chamber, inside the test cell (see also Platt et al., 2013). A fraction of the exhaust, sampled during the entire NEDC, was introduced into a smog chamber to study the aging of the mixture and SOA formation at 22 and −7 °C. A detailed description of the chamber and its experimental setup is presented in detail in Platt et al. (2013). The smog chamber is a 12.5 μm thick collapsible Teflon bag (DuPont Teflon fluorocarbon film (FEP), type 500A, Foiltec GmbH, Germany) with a volume of approximately 12 m^3 when full. The Teflon bag is suspended on an aluminum frame and illuminated by 40 UV lights (UV black lights Philips Ergoline Cleo-performance, peak emission at 350 nm, total power 4 kW) to simulate tropospheric photochemistry. The chamber is connected to a gas injection system which consists of a pure air generator (Atlas Copco SF 1 oil-free scroll compressor with 270 L container, Atlas Copco AG, Switzerland) equipped with an air purifier (AADCO 250 series, AADCO Instruments, Inc., USA). The vehicle emissions were injected into the chamber using a modified ejector dilutor (DI-1000, Dekati Ltd, Finland), equipped with a pressurized air heater (DH-1723, Dekati Ltd, Finland) applying a dilution factor of around 100–200. Around 2 μL (20 ppbv) of butanol-d9 is injected into the

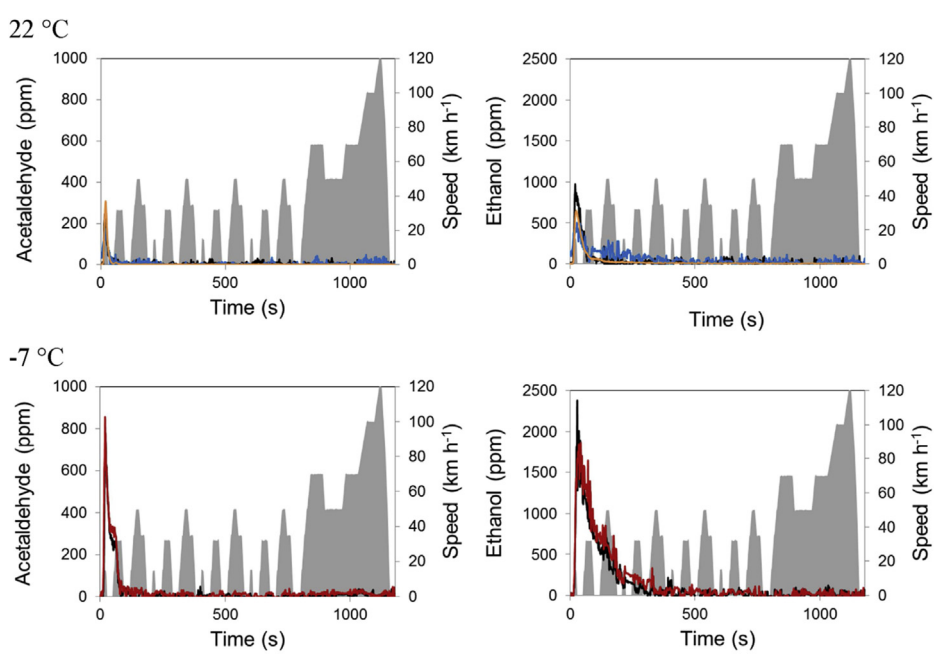

Fig. 2. Acetaldehyde and ethanol emission profiles over the NEDC (grey shadow) at 22 °C (top; blue Test 1, black Test 2 and orange Test 3) and −7 °C (bottom; black Test 4 and red Test 5). (For interpretation of the references to colour in this figure legend, the reader is referred to the web version of this article.)

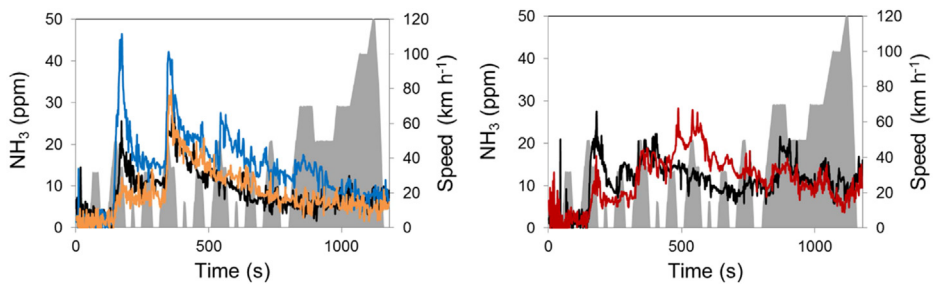

Fig. 3. NH_3 emission profiles over the NEDC (grey shadow) at 22 °C (left; blue Test 1, black Test 2 and orange Test 3) and −7 °C (right; black Test 4 and red Test 5). (For interpretation of the references to colour in this figure legend, the reader is referred to the web version of this article.)

chamber in order to assess photochemical aging times using the "OH clock" methodology described in Barmet et al. (2012). The butanol-d9 decay rate is monitored using a Proton Transfer Reaction Time-of-Flight Mass Spectrometer (PTR-ToF-MS 8000, Ionicon) and related to photochemical age via known reaction rate with OH. After a stabilization period, adjustment of the RH in the chamber and injection of O_3 to titrate initial NO to NO_2, continuous injection of nitrous acid (HONO) as additional OH radical source was started and the UV lights were switched on to initiate photochemistry. The HONO injection system is based on the continuous flow system described by Taira and Kanda (1990).

During the tests performed at 22 °C, the RH inside the smog chamber was held at either 40–50% (Test 1 and Test 2) or 80–90% (Test 3). Tests at −7 °C (Test 4 and Test 5) were performed at 40–50% RH. Particle size distribution and number concentration were measured inside the chamber with a scanning mobility particle sizer (SMPS) and a condensation particle counter (CPC, TSI 3076), respectively. Non-refractory condensed particle matter (compounds that vaporise at <~650 °C, e.g. organics, sulfate, nitrate) were monitored by a high resolution time of flight aerosol mass spectrometer (HR-ToF-AMS, Aerodyne, see DeCarlo et al., 2006), using a $PM_{2.5}$ inlet lens (Williams et al., 2013). Gas phase CO, THC, NOx, CO_2, H_2O, CH_4 (methane), and O_3 were measured with dedicated monitors (see Platt et al., 2013 for details). In the smog chamber, VOCs were analyzed by a PTR-ToF-MS. The instrument was operated in standard conditions, with a reaction chamber pressure fixed at 2.1 mbar, drift tube voltage and temperature at 500 V and 333 K, respectively, corresponding to an electric field strength applied to the drift tube (E) to buffer gas density (N) ratio of 125 Td. The data reduction procedure is fully described in Hellebust et al.. Briefly, 164 ions were identified in terms of their molecular formulas with a mass accuracy better than 20 ppm. These ions were then classified into families: aromatics, alcohols, acids, carbonyls or aliphatic hydrocarbons. In cases where the compound could neither be assigned to a chemical structure nor assigned to one of the families, it was classified according to its chemical formula either as an N-containing compound or an O-containing compound. For known compounds (benzene, toluene, acetaldehyde, etc) the concentration was calculated using the k values detailed in Cappellin et al. (2012). For ions with unknown rate constant, a default value of 3×10^{-9} cm^3 s^{-1} was used for oxygen-containing compounds and 2×10^{-9} cm^3 s^{-1} was used for compounds without oxygen in their formulas. Black carbon (BC) was monitored using an aethalometer (Aethalometer AE 33 beta, Aerosol d.o.o.) (Drinovec et al., 2014). Scanning mobility particle sizer (SMPS, custom built) data from the chamber were corrected for density, based on the particle chemical composition measured by the HR-ToF-AMS and subtracting BC, to provide a second measurement of the total non-refractory PM mass (i.e. those species quantified in the HR-ToF-AMS). This was used to correct for collection efficiency, CE, which was around 0.8 throughout all experiments. HR-ToF-AMS data were corrected for background CO_2 by calibrating the observed CO_2 in filtered air to external measurements using a cavity ring down spectrometer (Picarro, G2401).

3. Results and discussion

3.1. Regulated gaseous emissions

The emission factors (EFs; mass distance^{-1}) of the regulated gases obtained for a Euro 5a FFV tested over the NEDC, as well as the EFs over each of its two phases (UDC and EUDC), at 22 or −7 °C are summarized in Table 3. The FFV complied with Euro 5a emissions limits for the two temperatures studied (see Table 3). Notice that, in the test at −7 °C, known as type VI test (Directive 98/69/EC), Euro 5a regulation is limited to the urban part of the cycle (UDC) and only considers CO (15 g km^{-1}) and THC (1.8 g km^{-1}) emissions. CO emissions, over the entire NEDC, were more than 2 times higher for the tests performed at −7 °C than at 22 °C and THC, NMHC and NOx emissions were almost 4 times higher at −7 °C. The EFs of the regulated compounds were much higher during the urban part of the cycle (UDC) than over the extra urban (EUDC) (see Table 3), a similar behavior to that presented by other spark ignition vehicles fueled with gasoline (Dardiotis et al., 2013). This behavior, known as cold-start effect, is more pronounced for the tests performed at −7 °C mainly because catalyst light-off takes place later.

CO_2 emissions are not regulated by EU legislation for type approval emission tests. However, car manufacturers will have to ensure that their entire light duty vehicle fleet does not emit more than an average of 130 g km^{-1} of CO_2 by 2015 and 95 g km^{-1} by 2020. The FFV emitted 149 ± 2 g km^{-1} of CO_2 when tested at 22 °C, 20% less than emissions at −7 °C.

Similar THC, lower CO and higher NOx and CO_2 EFs were reported by Clairotte et al. (2013) for a Euro 4 and a Euro 5 FFV tested over the NEDC at 22 and −7 °C. Dardiotis et al. (2013) reported EFs of regulated gases and CO_2 for a series of Euro 5 (GLDVs) and diesel light duty vehicles (DLDV) tested over the NEDC at 22 and −7 °C. THC, NMHC, CO and CO_2 EFs of the GLDVs reported in that study were similar, within uncertainties, to those obtained for the FFV reported here. NOx EFs were up to 4 times higher for the GLDVs compared to the FFV. THC and CO emissions of the DLDVs studied by Dardiotis et al. were 2 times lower than those of the FFV (Dardiotis et al., 2013). However, NOx emissions were more than 20 times higher for the DLDVs than for the FFV.

3.2. Unregulated gaseous emissions

Table 3 summarizes the EFs of a number of atmospherically relevant unregulated compounds, obtained by online FTIR analysis of the FFV's exhaust at the tailpipe over the NEDC at 22 and −7 °C. A

Table 3
Regulated and unregulated emission factors (mg km^{-1}, *CO_2 emission factor (g km^{-1})) over the NEDC (bold) and its two phases (i.e. UDC and EUDC) at 22 and −7 °C. In parentheses, maximum semi-dispersion.

	22 °C			−7 °C			EF −7 °C/EF 22 °C
	NEDC	UDC	EUDC	NEDC	UDC	EUDC	
THC	**102** (±43)	273 (±7)	2.3 (±0.4)	**359** (±2)	954.6 (±0.1)	11 (±3)	3.5
CH_4	**13.5** (±0.3)	35.1 (±0.1)	0.9 (±0.2)	**38.4** (±0.6)	103 (±2)	1.0 (±0.1)	2.8
NMHC	**88** (±43)	238 (±7)	1.4 (±0.5)	**321** (±12)	852 (±26)	10 (±4)	3.6
NOx	**6.0** (±0.2)	11 (±2)	3.3 (±0.5)	**22.8** (±0.7)	55 (±3)	3.9 (±0.3)	3.8
CO	**413** (±40)	924 (±45)	115 (±1)	**893** (±23)	2152 (±104)	158 (±25)	2.2
CO_2^*g km^{-1}	**149** (±2)	195 (±4)	122 (±1)	**182** (±8)	249 (±15)	143 (±4)	1.2
N_2O	**0.4** (±0.1)	1.1 (±0.1)	0	**1.8** (±0.0)	2.6 (±0.0)	1.3 (±0.0)	4.1
NH_3	**4.6** (±0.2)	7.1 (±0.8)	3.2 (±0.1)	**6.4** (±0.0)	7.1 (±0.7)	6.0 (±0.3)	1.4
Ethanol	**54** (±17)	108 (±48)	22 (±2)	**245** (±24)	351 (±66)	183.3 (±0.5)	4.5
Acetaldehyde	**12.7** (±0.0)	20 (±3)	8 (±2)	**43** (±7)	48 (±9)	39.9 (±0.3)	3.4
Formaldehyde	**1.8** (±0.0)	3.6 (±0.2)	0.7 (±0.1)	**3.4** (±0.3)	4.8 (±0.6)	2.6 (±0.1)	1.9
Ethylene	**6** (±1)	15 (±2)	1.2 (±0.1)	**29** (±2)	42 (±4)	21.9 (±0.2)	4.7
Ethane	**1.4** (±0.0)	3.5 (±0.0)	0.3 (±0.1)	**4.1** (±0.2)	6.0 (±0.1)	3.0 (±0.2)	2.8
Acetylene	**2.7** (±0.2)	5.8 (±0.8)	0.9 (±0.1)	**17** (±1)	24 (±4)	13.2 (±0.1)	6.4
Toluene	–	–	–	**5.9** (±0.2)	71.8 (±8)	–	
Benzene	–	–	–	**3.6** (±0.2)	43.9 (±6)	–	

comprehensive analysis was performed with respect to the exhaust emissions of: formaldehyde and acetaldehyde, classified as human carcinogen and as probable carcinogenic, respectively by the US Department of Health and Human Services; ammonia (NH_3), which is a precursor of atmospheric secondary aerosols (Pope et al., 2002; Behera and Sharma, 2010) and is also classified under the European dangerous substances directive (67/548/EEC) as toxic, corrosive and dangerous for the environment; ethanol, precursor of acetaldehyde and PAN in the atmosphere; (Millet et al., 2012a, 2010) and two greenhouse gases (GHG), nitrous oxide (N_2O) and methane (CH_4). The emissions of toluene and benzene were also monitored. Note that the aromatics content (% vol) in E5 gasoline is approximately 31%, and about 4.5 and 7.5% in the E85 and E75 ethanol blends, respectively. While emissions of benzene or toluene were below FTIR detection limits at 22 °C, 3.6 and 5.9 (±0.2) mg km^{-1} of benzene and toluene were emitted at −7 °C (see Table 3). The cold-start operation of spark ignition vehicles is typically associated with rich combustion to avoid misfires due to condensation effects on the cylinder. The enrichment of the air/fuel mixture during cold-start operation results in incomplete fuel combustion, leading to higher CO and HC emissions during cold-start (Dardiotis et al., 2013). Moreover, since three-way catalysts (TWC) require a certain temperature (typically above 300 °C) to work at full efficiency, emissions are significantly higher until the catalyst reaches the optimal working conditions (Millet et al., 2012b). At lower ambient temperatures, the engine and catalyst take longer to warmup, which results in higher emissions.

The emissions of the unregulated compounds were higher at −7 °C than at 22 °C over the NEDC, as it was in the case for the regulated compounds. Emission factors of most unregulated compounds were also substantially higher over the UDC than over the EUDC. The only exception was ammonia, with slightly higher emission during the UDC. However, once the catalyst reached the optimal operating temperature, the other unregulated compounds were essentially under the limits of detection. At −7 °C the catalyst light-off takes longer (see Fig. 2), as a consequence, compounds such as acetaldehyde, ethanol and other VOCs are emitted for a longer period, which in some cases reached the phase 2 (EUDC) of the cycle as reflected in Table 3. The emission profiles of ethanol and acetaldehyde at both temperatures can be seen in Fig. 2.

Table 3 shows that EFs of ethanol were more than 4 times higher for tests performed at −7 °C than at 22 °C. Clairotte et al. (2013) reported similar ethanol EFs for a Euro 5a tested at 22 °C but at −7 °C, ethanol EFs reported were 2 times higher than those of our FFV. The acetaldehyde/formaldehyde mass ratio obtained (~6) is consistent with those measured in cities where ethanol blends are widely used (Grosjean et al., 2002).

Acetaldehyde, a product of the incomplete oxidation of ethanol, presented a similar emission profile to that of ethanol, i.e. emissions at −7 °C were higher (3 times) than at 22 °C, with abundant emissions still present during the EUDC at −7 °C (see Table 3). Formaldehyde EFs were approximately 2 times higher at −7 °C. EFs of formaldehyde were similar to those reported in previous studies (Clairotte et al., 2013). EFs of acetaldehyde were similar to those reported by Westerholm et al. (2008) but lower than those reported by Clairotte et al. (2013).

In spark ignition vehicles, NH_3 is formed in the TWC after catalyst light-off (Whittington et al., 1995; Huai et al., 2003; Bradow and Stump, 1977), through a mechanism that involves NO and H_2, and continues for the entire duration of the tests. Molecular hydrogen is produced from a water–gas shift reaction between CO and water or via steam reforming from hydrocarbons (Whittington et al., 1995). NH_3 formation over the catalyst is enhanced at low air/fuel ratios, also known as rich combustion, where conditions are reductive and higher concentrations of CO and H_2 are present (Whittington et al., 1995; Heeb et al., 2010). These are typical conditions during the accelerations, which explain the higher emissions of NH_3 during the acceleration events present in the cycle (see Fig. 3). NH_3 emissions will then depend on driving mode and combustion enrichment. Hence, higher NH_3 emissions are expected for an aggressive or dynamic driving style, where accelerations (rich combustion) and decelerations (lean combustion) take place more often (Huai et al., 2003). The NH_3 EFs were consistent with the literature for other Euro 5 spark ignition vehicles (Kean et al., 2009; Livingston et al., 2009; Suarez-Bertoa et al., 2014).

The emissions of NH_3 were affected by low ambient temperatures since the vehicle runs under rich conditions (air/fuel ratio < 1) for a longer period at low temperature than at 22 °C. As a consequence, the emissions of NH_3 at −7 °C were 1.4 times higher than at 22 °C.

Table 3 shows that N_2O emissions were affected by low ambient temperature, increasing from 0.4 mg km^{-1} at 22 °C to 1.8 mg km^{-1} at −7 °C, which is in agreement with previous studies (Graham et al., 2008). N_2O is catalytically produced, especially at colder catalyst temperatures, consistent with larger observed emissions during the UDC. Similar N_2O EFs were reported by Clairotte et al. (2013) at 22 °C. However, they reported N_2O emissions 6 times

lower at −7 °C than here. Graham et al. (2009) reported median N_2O EFs equal to 1 and 12 mg km^{-1} for a series of GLDVs and DLDV, respectively.

CH_4 EFs were 3 times higher at −7 °C than at 22 °C. As reflected in Table 3, the UDC accounts for almost all the CH_4 emissions at both temperatures. Overall, CH_4 and N_2O emissions, with their global warming potential (25 and 298 eq g CO_2 over 100 years for CH_4 and N_2O, respectively), were responsible for a 0.5 g km^{-1} and 1.5 g km^{-1} increase in terms of CO_2 equivalent emissions at 22 and −7 °C, respectively. FFV CH_4 emissions were similar to those of GLDV reported by Dardiotis et al. (2013).

3.3. Ozone formation potential

The estimated OFPs (mg O_3 km^{-1}) and the percentage contributions of a group of compounds emitted by the FFV over the NEDC at 22 and −7 °C are illustrated in Fig. 4. The columns in Fig. 4 represent the total OFP and show the contribution of each compound considered. This group of compounds accounted for more than 90% of the THC mass at 22 °C, and nearly 100% (within the uncertainties of the instruments) at −7 °C. Besides CO, the compounds used for the estimation of these OFPs are mainly emitted during the cold-start. At −7 °C, the calculated OFPs were 4 times higher than that those obtained at 22 °C.

As illustrated in Fig. 4, acetaldehyde, ethylene and their precursor, ethanol, were the main contributors to the OFP, accounting for up to 90% of the total at both temperatures. As a consequence of increased use of ethanol fuel in Brazil, acetaldehyde, associated with emissions from FFVs, has become the fourth largest ozone precursor in some Brazilian areas (Corrêa et al., 2010), demonstrating that the fuel used by a big part of a city's vehicular fleet could dominate the urban atmospheric composition. The studied FFV presented an OFP 1.6 times higher than that reported for two flex-fuel vehicles by Graham et al. (2008). When comparing the FFV with modern gasoline and diesel vehicles from the literature, it can be observed that OFPs are affected by the compounds directly related to the high concentration of ethanol present in the E85 and E75 blends, and to a large extent by low ambient temperatures. In fact, the OFPs at 22 °C were 5 times and 1.6–5 times higher than those reported by Clairotte et al. (2013) and Adam et al. (2011) respectively.

3.4. Photochemical aging of emissions

Fig. 5 illustrates the composition of the fresh and aged mixtures measured at the smog chamber by the PTR-ToF-MS at the studied temperatures. FFV emissions were dominated by a mix of carbonyls and alcohols. In the smog chamber, carbonyls and alcohols accounted for about 60% and 65% of the total HC volume measured by the PTR-ToF-MS, at 22 and −7 °C, respectively. This is in contrast to a previous smog chamber study on GLDVs and DLDVs where emissions were dominated by aromatics and aliphatic hydrocarbons, and carbonyls only, respectively (Hellebust et al. in prep).

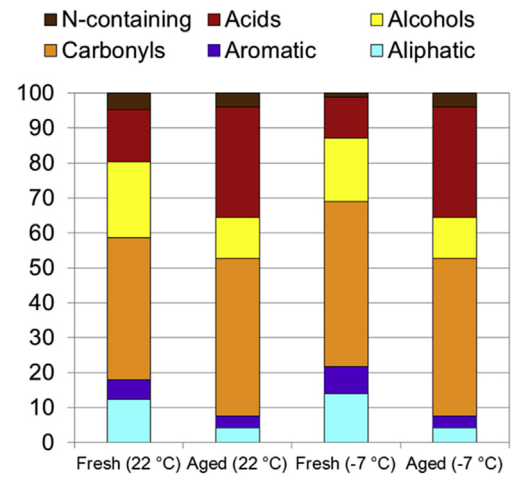

Fig. 5. Composition of the fresh and aged (after 10 h equivalent OH exposure) mixtures measured at the smog chamber by PTR-ToF-MS at 22 °C (Test 1) and −7 °C (Test 4), broken down by chemical families.

The proton affinity of ethane (596 kJ mol^{-1}), ethylene (641 kJ mol^{-1}) and acetylene (641 kJ mol^{-1}) are lower than that of water (about 697 kJ mol^{-1}). Therefore, these NMHCs could not be measured in the smog chamber using the PTR-ToF-MS. Using the FTIR measurements made at the vehicle tailpipe, it was estimated that they accounted for 11% and 15% of the total NMHC measured by the FFV during the tests at 22 and −7 °C, respectively.

In the aged mixtures (see Fig. 5), the organic acids made up 40% of the total, and the carbonyls up to 48%, indicative of a well processed system. In the fresh mixtures, acetaldehyde ($C_2H_5O^+$) and formaldehyde (CH_3O^+) were the main carbonyls observed. In contrast, in the aged mixtures, ions with the assigned ionic formula $C_3H_7O^+$, $C_3H_5O_2^+$, and $C_4H_7O_2^+$, tentatively identified as propanal or/and acetone, methylglyoxal and dimethylglyoxal, respectively, represented more than 30% of the carbonyl family. The main organic acids observed in the aged mix were formic ($CH_3O_2^+$) and acetic acids ($C_2H_5O_2^+$) and represented 11% and 30% ($CH_3O_2^+$ and $C_2H_5O_2^+$) of the total mass at 22 °C and 8% and 18% ($CH_3O_2^+$ and $C_2H_5O_2^+$) at −7 °C.

Fig. 6 illustrates the evolution of a series of organic compounds measured at the smog chamber after stabilization of the FFV exhaust as a function of the time after lights on. It can be seen that while the concentration of ethanol ($C_2H_7O^+$) decreased with aging time, the concentration of the oxidation products acetaldehyde, formaldehyde, formic and acetic acid, methylglyoxal and

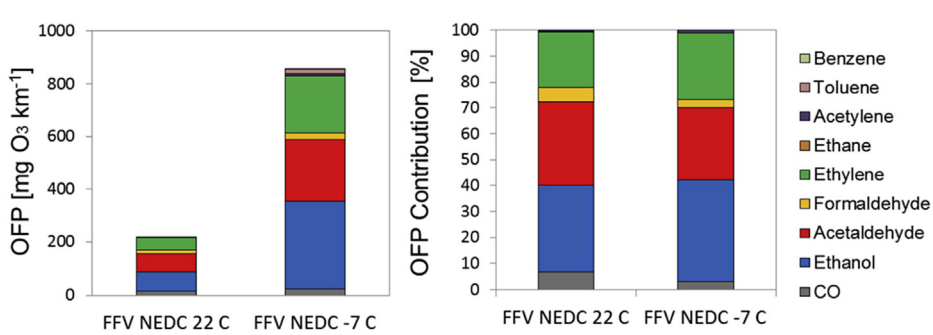

Fig. 4. Estimated OFPs (mg O_3 km^{-1}) (left) and the percentage contributions (right) at 22 and −7 °C over the NEDC.

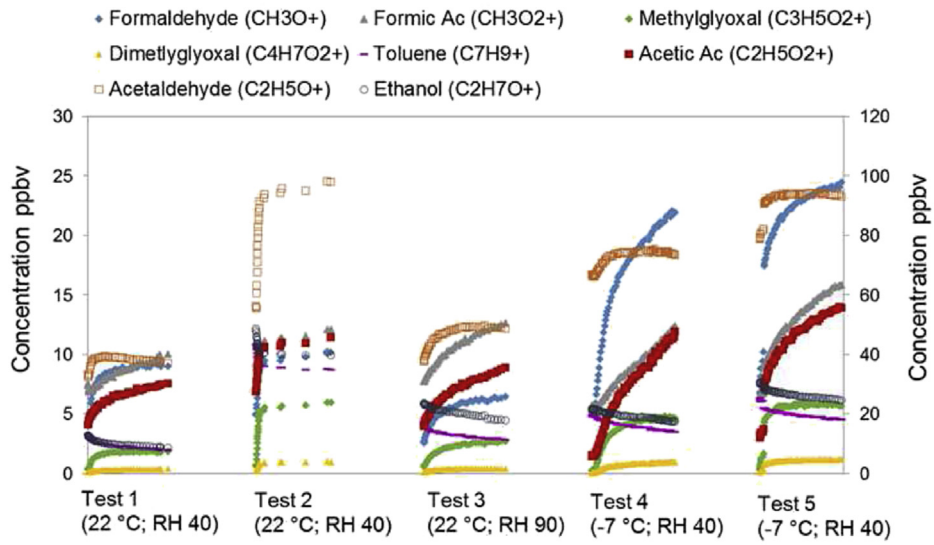

Fig. 6. Progression inside the smog chamber of the main species contained in the exhaust mixtures and the reaction products, for the tests at 22 and −7 °C, as a function of time after lights-on measured by PTR-ToF-MS. Each test represents 10 h equivalent OH exposure. On the right axis, concentration (ppbv) of acetic acid ($C_2H_5O_2^+$), acetaldehyde ($C_2H_5O^+$) and ethanol ($C_2H_7O^+$).

dimethylglyoxal, increased.

The presence of the ions $C_5H_9O^+$, $C_3H_9O_2^+$, $C_4H_9O_2^+$, which could correspond to pentenone, 1-ethoxy-metan-1-ol, ethyl acetate (see Table 4), after aging, suggests that a series of non-radical reactions (aldol condensation, Claisen condensation, acetylation, Baeyer-Villiger oxidation) involving ethanol, acetaldehyde, formaldehyde could have taken place. Moreover, methylglyoxal and dimethylglyoxal could lead to polymerization processes, as suggested by Kalberer et al. (2006). Altieri et al. (2008) and Tan et al., (2010) reported that methylglyoxal oxidation by OH radicals could also lead to high molecular weight compounds and carboxylic acids that are found predominantly in the particle phase.

3.5. Secondary organic aerosol formation

Table 5 summarizes the FFV emission factors of BC and POA and SOA formation potential in mass carbon (C) per mass of fuel units at 22 and −7 °C. Fig. 7 shows the concentration of the carbonaceous condensed phase (mass per mass of fuel units) measured at the smog chamber after the injection of the FFV exhaust as a function of the time after irradiation at 22 and −7 °C.

Primary emissions (BC and POA) are taken from the average concentrations measured before lights on. Absolute masses of both primary and secondary components are converted into emission factors (potential of production, for secondary species) per mass of fuel (EF_{MASS}, right axes) using a chemical mass balance approach (adapted from Phuleria et al., 2006):

$$EF_{\mathrm{Mass}} = \frac{\Delta P}{\Delta C_{CO_2} + \Delta C_{CO} + \Delta C_{HC}} \times WC \quad (1)$$

where P is the mass of a pollutant, C denotes the carbon mass from CO_2, CO, gas phase hydrocarbon (HC), particle phase organic carbon (OC) from aerosol mass spectrometer measurements analysis, and BC. WC is the fuel carbon content for the fuel blends used (0.604 and 0.574 for E75 and E85 blends respectively; see Table 5).

The observed increase in aerosol concentration after wall loss correction is considered to represent the SOA production. Wall loss correction factors were derived from the decay of the black carbon mass (Aethalometer, 880 nm channel). The organic aerosol concentration C_{OA} was corrected for wall losses ($C_{OA,WLC}$) assuming material lost to the walls does not partition via (e.g. Hildebrandt et al., 2009):

$$C_{OA,WLC} = C_{OA,SUSP.}(t) + \int_0^t k(t) \times C_{OA,SUSP.}(t)d(t) \quad (2)$$

where the $C_{OA,SUSP}$ is the observed OA concentration at time = t and an exponential decay constant k taken from an exponential fit of BC as a function of time after lights on (average particle half-life is 2.2 ± 0.6 h).

Table 4
Exact mass and molecular formulas of the main ions measured by the PTR-Tof-MS, together with the most probable compound that corresponds to the obtained ion mass.

m/z	Protonated ion	Most probable compound
31.0178	CH_3O^+	Formaldehyde
45.0337	$C_2H_5O^+$	Acetaldehyde
47.0125	$CH_3O_2^+$	Formic acid
47.0486	$C_2H_7O^+$	Ethanol
59.0481	$C_3H_7O^+$	Propanal; acetone
61.0277	$C_2H_5O_2^+$	Acetic acid; glycoaldehyde
73.0279	$C_3H_5O_2^+$	Methylglyoxal
85.065	$C_5H_9O^+$	Pentenone; pentenal
77.0532	$C_3H_9O_2^+$	1-ethoxy-metan-1-ol
87.044	$C_4H_7O_2^+$	Dimethylglyoxal
89.0589	$C_4H_9O_2^+$	Ethyl acetate
93.0698	$C_7H_9^+$	Toluene

Table 5
Emission factors (units 10^{-3} g C kg^{-1}) of BC and POA, and SOA production after 10 h of aging in the mobile smog chamber.

Test	T °C	RH %	BC	POA	SOA	SOA/BC	SOA/POA	SOA/(POA + BC)
Test 1	22	40	0.4	0.4	2.3	5	6	3
Test 2	22	40	0.3	0.4	3.0	10	7	4
Test 3	22	90	0.4	0.1	1.3	3	13	3
Test 4	−7	40	4.5	1.0	13.4	3	14	2
Test 5	−7	40	5.1	4.9	38.2	8	8	4

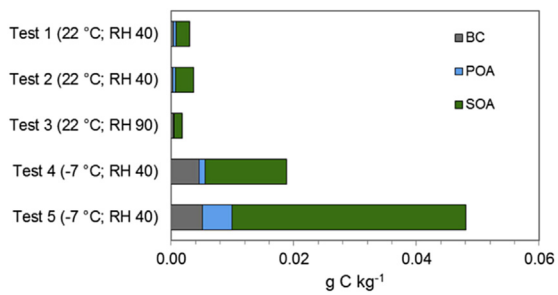

Fig. 7. Emission factors (g C kg^{-1}) of BC (grey) and POA (blue), and SOA (green) production from the FFV's emissions measured after aging in the mobile smog chamber. (For interpretation of the references to colour in this figure legend, the reader is referred to the web version of this article.)

The wall loss characteristic time (1/k, Eq. (2)) before switching on the lamps is very similar to the one after, also based on our previous results (Platt et al., 2013; Zardini et al., 2014).

Fig. 8 illustrates how gas-phase processing of the FFV exhaust results in SOA formation at 22 and −7 °C. The presented SOA was formed after an OH exposure that corresponds to 10 h of atmospheric aging assuming a global annual mean OH concentration of 10^6 molecules cm^{-3} (Prinn et al., 2001), suggesting that SOA formation, from this type of mixture, is a fast process in the atmosphere even at low temperatures. Fig. 9 displays the wall-loss corrected concentration and emission factor of the organic aerosol in the smog chamber as a function of the time after irradiation and OH exposure at 22 °C together with the concentration of BC and POA. Table 5 shows that, as for spark ignition vehicles (Mathis et al., 2005), primary emissions increase at lower temperatures. Hence, EFs of BC were 11–17 times larger at −7 °C than at 22 °C, and EFs of POA were 3–12 times higher at −7 °C compared to 22 °C. Furthermore, SOA was 4–16 times higher at −7 °C than at 22 °C. Analogously to GLDVs reported in previous studies (Platt et al., 2014; Gordon et al., 2014a), the FFV's aged exhaust produced more secondary organic mass than primary emissions, emphasizing the importance of secondary pollutants for a full understanding of vehicle emissions. SOA was 3–10 times larger than BC mass, 6 to 24 times larger than POA mass, hence, about 3 times larger than the total primary emissions (BC + POA) (see Table 5). The relatively low primary emissions have been attributed to the difference in physico-chemical properties of the ethanol blend, being the oxygen content in the fuel the primary contributing factor for lowering particulate emissions, by affecting combustion kinetics (Karavalakis et al., 2014). SOA formation is very sensitive to ambient conditions, and very small variations in e.g. temperature, OH concentration, chamber surface/volume, RH, organic aerosol loading, VOC/NOx ratio, and emission composition etc. will add up to produce the relatively large variations observed. It should be understood that the reported SOA formation does not represent an absolute value (the real atmosphere is extremely variable), rather, possible values under plausible conditions. The increase in aerosol mass was mostly due to condensation of new material on pre-existing seed particles, the primary emission (see Fig. S2 in the supplementary material). The largest part of the aerosol was between 100 and 500 nm in all experiments, indicating that particles were within the transmission window of the AMS. Test 3 (22 °C and smog chamber at 90% RH) resulted in similar EFs and composition of the gaseous emissions to Test 1 and Test 2 (22 °C and smog chamber at 40% RH). While similar BC emissions were measured in the smog chamber for the three tests at 22 °C, POA emissions and SOA formation were lower for Test 3 than for Test 1 and Test 2. Nonetheless, the SOA (BC + POA) ratio resulted to be similar for the three tests (see Table 5). The divergence of SOA formation observed for Test 1 and Test 2 was slightly higher than the one observed between Test 1 and Test 3. For all these reasons, and the absence of further tests at 90% RH, we could not assess if different RH in the smog chamber leads to different SOA formation. Therefore, only Test 1 and Test 2 are discussed.

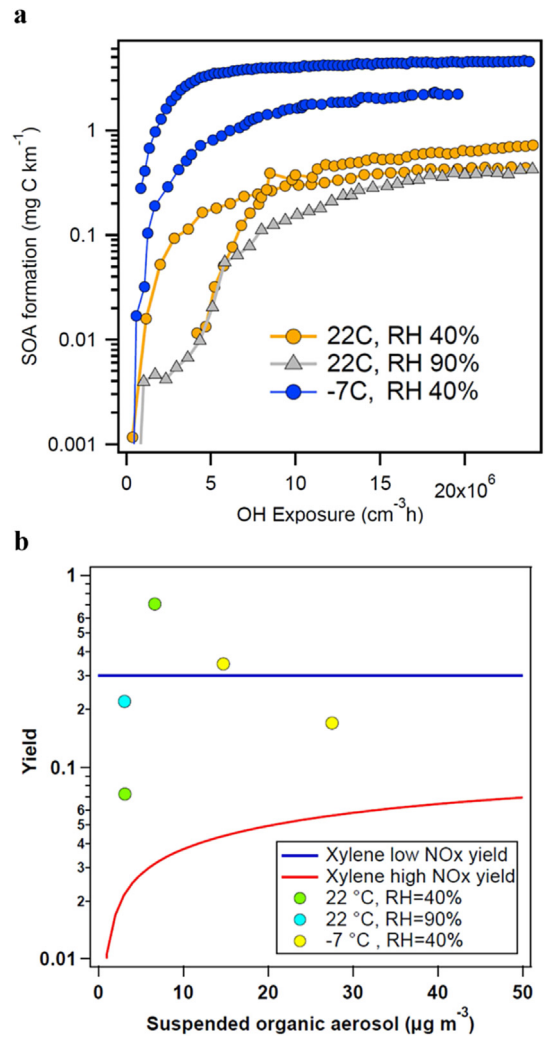

Fig. 8. (a) Observed secondary aerosol formation (wall-loss corrected) in the smog chamber during aging of the FFV's emissions at 22 °C and 40% RH (yellow), 22 °C and 90% RH (grey) and −7 °C and 40% RH (blue). (b) Apparent SOA mass yield as a function of suspended OA concentration (C_{OA}) per reacted aromatics mass. Maximum (low NOx) and minimum (high NOx) SOA yields for m-xylene are shown as blue and red line, respectively. (For interpretation of the references to colour in this figure legend, the reader is referred to the web version of this article.)

The measured primary aerosol emissions were substantially lower than those previously reported for a Euro 5 and series of LEV I and LEV II GLDV (Platt et al., 2013; Gordon et al., 2014a) but higher than those measured from a series of heavy duty diesel vehicles (HDDVs) equipped with diesel particle filter (DPF) system (Gordon et al., 2014b). At 22 °C, the FFV presented lower SOA production than those from the Euro 5 reported by Platt et al. (2013) and the series of LEV I and LEV II GLDVs reported by Platt et al. (2013) and Gordon et al. (2014a). The SOA formed from the exhaust of the FFV at 22 °C was two orders of magnitude lower than from the Euro 5 GLDV (Platt et al., 2013) and one order of magnitude lower than those reported for the LEV I and LEV II GLDVs (Gordon et al., 2014a).

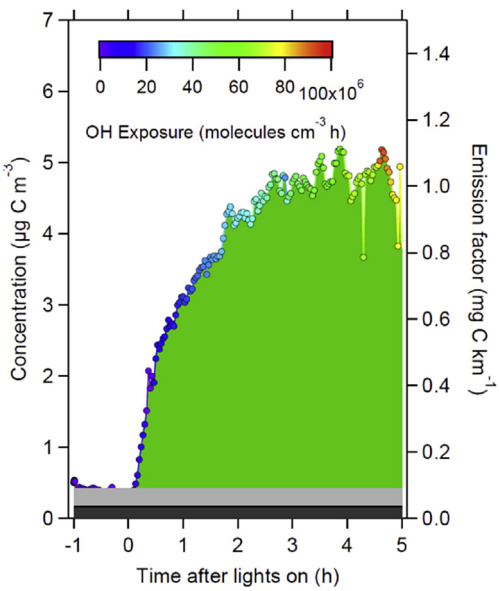

Fig. 9. Development of organic aerosol mass in the smog chamber as a function of the time after irradiation (x axis) and OH exposure (color legend) at 22 °C. Dark grey illustrates black carbon, light grey primary organic carbon and green secondary organic carbon. The presented is wall-loss corrected data. (For interpretation of the references to colour in this figure legend, the reader is referred to the web version of this article.)

However, SOA formation from the FFV was two times larger than those reported for the HDDVs equipped with a DPF (Gordon et al., 2014b). Higher SOA formation from gasoline vehicles exhaust may be due to the larger emissions of aromatic compounds and other heavier hydrocarbons. On the other hand, the difference in SOA formation between the FFV and the HDDVs equipped with a DPF could be explained in terms of differences in the magnitude of THC emissions, which are typically higher for spark ignition vehicles than for modern diesel vehicles. Furthermore, Gordon et al. (2014b) showed that catalyzed DPFs are very effective in reducing both primary particulate emissions and SOA production (Gordon et al., 2014b).

The O:C ratio of the fresh and aged organic aerosol (OA) rapidly increased with OH exposure. The increase of the O:C ratios indicates the addition of oxygenated organics to the aerosol (Platt et al., 2013; Jimenez et al., 2009; Ng et al., 2010). The O:C ratio observed for the aged OA at 22 °C is in the range (~0.7) of ambient low-volatility oxygenated organic aerosol (LV-OOA) observed by Ng et al. (2010) and it is also similar to that reported for a Euro 5 GLDV by Platt et al. (2013). At −7 °C, the O:C ratio measured for the aged OA was slightly lower, 0.5.

The contribution of the aromatics to SOA formation was estimated by calculating an apparent aerosol yield, y_{apparent}, assuming that all SOA comes from aromatic precursors, as described in Platt et al. (2014):

$$y_{\text{apparent}} = C_{SOA} \Big/ \sum_i \Delta i \qquad (3)$$

where C_{SOA} is the SOA produced (µg m^{-3}) for a given mass change in aromatic i (Δi, i = benzene, toluene or C_2–C_4 alkylated benzenes). Calculated apparent yields were well above the SOA yields for m-xylene, a major aromatic constituent of gasoline, considering a high NOx scenario, indicating that most SOA must be from non-aromatic precursors (Fig. 8). We assume high NOx as considerable NO_2 was present during all experiments, ensuring the presence of some NO via photolysis (see e.g. Platt et al., 2014). Furthermore, a constant stream of HONO was injected (see experimental section) which also photolyses to produce NO. Similar conclusions were drawn from a gasoline vehicle whose fuel contained ~5 times more aromatics than the ethanol blends used here (Platt et al., 2013). The obtained SOA apparent yields (about 0.1–0.4 at 10^6 h cm^3 OH exposure and 10 µg m^{-3} loading) were in the same range of those reported for gasoline vehicles emissions by Gordon et al. (2014a). Due to uncertainties in yield estimates in our study and in Gordon et al. (2014a), it is not clear whether the non-aromatic SOA precursors present in gasoline and in ethanol blends emissions are the same or whether additional precursors present in flex-fuel vehicles emissions, such as oxygenated compounds, may play a role in SOA formation. An unambiguous determination of SOA precursors for both gasoline and ethanol flex-fuel exhaust emissions would require further study.

Fig. 10 shows examples of the obtained high resolution mass spectra. The top panel spectra are a good representation of hydrocarbon-like organic aerosol (HOA) presenting typical hydrocarbon signatures (Ng et al., 2010) dominated by the series C_nH_{2n+1} and C_nH_{2n-1} (m/z 27, 29, 41, 43, 55, 57 …). The bottom panel spectra show high 44/43 ratios (ratio of the ions m/z 44 and m/z 43) which is commonly related to low-volatility oxygenated organic aerosol (LV-OOA). The oxygenated organic aerosol (OOA) component is distinguished by the prominent m/z 44 (CO_2^+) in its spectrum and the lower intensity of higher mass fragments. Very few oxygenated fragments are present at high m/z of the aged OA mass spectra at both temperatures, which indicates the possible prevalence of oligomers.

The fraction 44:43 (m/z:m/z) of the aged OA is lower (2 times) at −7 °C than at 22 °C. The total concentration of the organic acids, measured by PTR-ToF-MS is 40% higher at −7 °C than at 22 °C.

The higher concentration of regulated and unregulated compounds present at −7 °C than at 22 °C resulted in more SOA at −7 than at 22 °C. The reason could be a drop of the saturation vapor pressure of the reaction products, which, at 22 °C were in the gas phase while at −7 °C may be in the condensed phase, or the higher concentrations of reacting compounds which could lead to formation of high molecular weight compounds, including oligomers (Kalberer et al., 2006). The lower O:C ratio at −7 °C may suggest the formation of oligomers by aldol condensation which leads to the loss of H_2O (Reinhardt et al., 2007) and/or the above mentioned condensation of additional organics at the low temperature.

4. Conclusions

The results obtained in our study show that widespread use of vehicles running on high ethanol-content fuel blends, E85 and E75, needs to be thoroughly evaluated due to the negative effects that their emissions may have on urban air quality.

The flex-fuel vehicle (FFV) studied here complied with Euro 5a emission regulations. However, high emissions of ethanol (54 (±17) and 245 (±24) mg km^{-1}, at 22 and −7 °C, respectively) and toxic and harmful compounds such as acetaldehyde (12.7 (±0.0) and 43 (±7) mg km^{-1}, at 22 and −7 °C, respectively), ammonia (4.6 (±0.2) and 6.4 (±0.0) mg km^{-1}, at 22 and −7 °C, respectively) were measured. Emissions factors of all the compounds studied increased at the lower temperature. The FFV emissions resulted in a high ozone formation potential (OFP), which was nearly 4 times higher at lower temperature (218 and 860 mg O_3 km^{-1} at 22 and −7 °C, respectively).

The studied system presented a reaction mixture of short-chain VOCs (mainly ethanol and acetaldehyde), which, after aging led into a highly oxidized aerosol, with O:C ratio 0.5–0.7. SOA was one order of magnitude higher at −7 °C (13.4–38.2 10^{-3} g C kg^{-1} and 1.3–3.0 10^{-3} g C kg^{-1} at −7 and 22 °C, respectively). These results

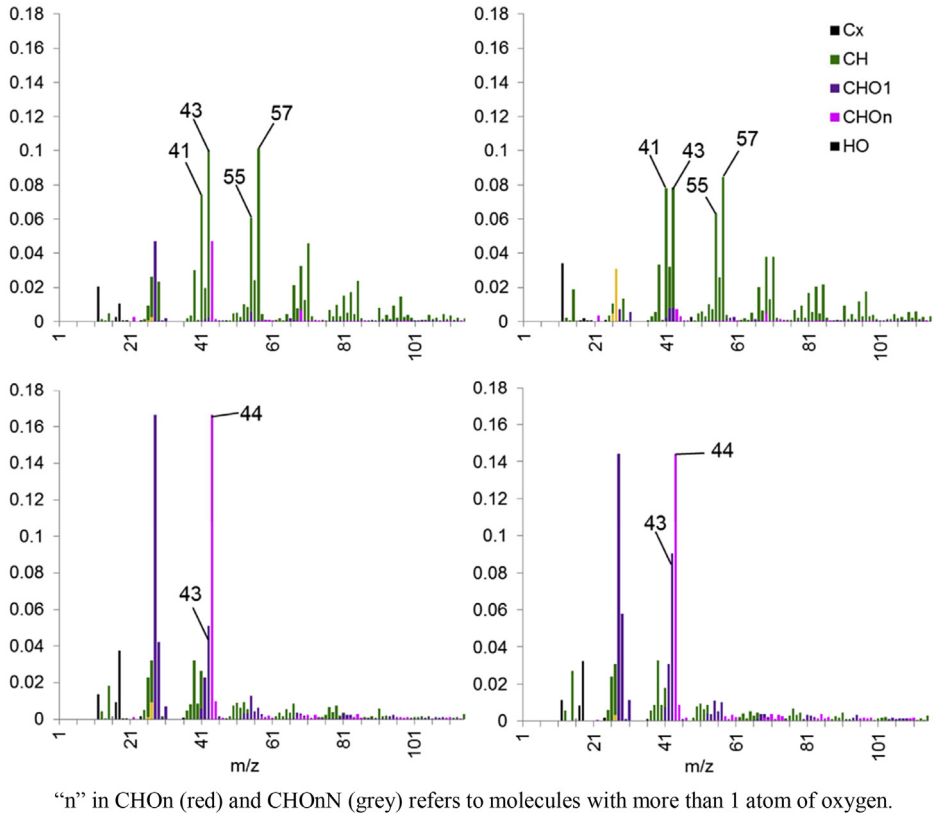

Fig. 10. Example of the high resolution mass spectra measured from the smog chamber of the emitted fresh (top panel) and 10 h aged (bottom panel) organic aerosol. Top and bottom left correspond to the test performed at 22 °C. Top and bottom right correspond to a test performed at −7 °C.

show that SOA formation from vehicular exhaust can arise from the reaction and/or oxidation of small functionalized molecules such as acetaldehyde and ethanol and not only from aromatics, as it is often hypothesized.

In the present study, SOA was, on average, 3 times larger than total primary emissions (BC + POA) at both, 22 and −7 °C. Therefore, at the time being, and as for gasoline vehicles, vehicular PM regulation would neglect the largest fraction of the total PM emitted and formed from the FFVs.

As it is often observed for the spark ignition vehicles, most of the THC emissions (>90%) occurred before the catalyst light off, during the cold-start. Therefore, a shorter time until vehicle catalyst light-off is needed to reduce THC emissions, which act as SOA and O_3 precursors.

The use of flex-fuel vehicles with high ethanol content fuel blends is being promoted in regions like northern Europe, where very low temperature is a common scenario. The extensive use of these vehicles at low temperature will result in high emissions of ethanol and acetaldehyde that may lead to large formation of O_3 and SOA.

Disclaimer

The opinions expressed in this manuscript are those of the authors and should in no way be considered to represent an official opinion of the European Commission.

Acknowledgments

The VELA staff is acknowledged for the skilful technical assistance, in particular M. Cadario, R. Colombo, G. Lanappe, P. Le Lijour, F. Muehlberger, and M. Sculati as well as Rene Richter from PSI. We acknowledge the financial support by the Swiss Federal Office for the Environment (FOEN), the Swiss Federal Roads Office (FEDRO) and the Swiss National Science Foundation (SAPMAV 200021_13016). The authors also acknowledge the MASSALYA instrumental platform (Aix Marseille Université, lce.univ-amu.fr) for the provision of the PTR-ToF-MS measurements used in this publication and the French Environment and Energy Management Agency (ADEME, Grant numbers 1162C0002 and 1262C0017).

Appendix A. Supplementary data

Supplementary data related to this article can be found at http://dx.doi.org/10.1016/j.atmosenv.2015.07.006.

References

Adam, T.W., Astorga, C., Clairotte, M., Duane, M., Elsasser, M., Krasenbrink, A., Larsen, B.R., Manfredi, U., Martini, G., Montero, L., Sklorz, M., Zimmermann, R., Perujo, A., 2011. Atmos. Environ. 45, 2842–2848.
Altieri, K.E., Seitzinger, S.P., Carlton, A.G., Turpin, B.J., Klein, G.C., Marshall, A.G., 2008. Atmos. Environ. 42, 1476–1490.
Andrade, J. B. d., Andrade, M.V., Pinheiro, H.L.C., 1998. J. Braz. Chem. Soc. 9, 219–223.
Atkinson, R., Baulch, D.L., Cox, R.A., Crowley, J.N., Hampson, R.F., Hynes, R.G., Jenkin, M.E., Rossi, M.J., Troe, J., 2006. Atmos. Chem. Phys. 6, 3625–4055.
Barmet, P., Dommen, J., DeCarlo, P.F., Tritscher, T., Praplan, A.P., Platt, S.M., Prévôt, A.S.H., Donahue, N.M., Baltensperger, U., 2012. Atmos. Meas. Tech. 5, 647–656.
Behera, S.N., Sharma, M., 2010. Sci. Total Environ. 408, 3569–3575.
Bradow, R.L., Stump, F.D., 1977. SAE Technical Paper No. 770369.
Cappellin, L., Karl, T., Probst, M., Ismailova, O., Winkler, P.M., Soukoulis, C., Aprea, E., Märk, T.D., Gasperi, F., Biasioli, F., 2012. Environ. Sci. Technol. 46, 2283–2290.
Carter, W.P.L., 1994. Air Waste 44, 881–899.
Chemical Summary for Acetaldehyde, U.S.Environmental Protection Agency Washington, DC.
Clairotte, M., Adam, T.W., Chirico, R., Giechaskiel, B., Manfredi, U., Elsasser, M.,

Sklorz, M., DeCarlo, P.F., Heringa, M.F., Zimmermann, R., Martini, G., Krasenbrink, A., Vicet, A., Tournié, E., Prévôt, A.S.H., Astorga, C., 2012. Anal. Chim. Acta 717, 28–38.
Clairotte, M., Adam, T.W., Zardini, A.A., Manfredi, U., Martini, G., Krasenbrink, A., Vicet, A., Tournié, E., Astorga, C., 2013. Appl. Energy 102, 44–54.
Cook, R., Phillips, S., Houyoux, M., Dolwick, P., Mason, R., Yanca, C., Zawacki, M., Davidson, K., Michaels, H., Harvey, C., Somers, J., Luecken, D., 2011. Atmos. Environ. 45, 7714–7724.
Corrêa, S.M., Martins, E.M., Arbilla, G., 2003. Atmos. Environ. 37, 23–29.
Corrêa, S.M., Arbilla, G., Martins, E.M., Quitério, S.L., de Souza Guimarães, C., Gatti, L.V., 2010. Atmos. Environ. 44, 2302–2308.
Dardiotis, C., Martini, G., Marotta, A., Manfredi, U., 2013. Appl. Energy 111, 468–478.
DeCarlo, P.F., Kimmel, J.R., Trimborn, A., Northway, M.J., Jayne, J.T., Aiken, A.C., Gonin, M., Fuhrer, K., Horvath, T., Docherty, K.S., Worsnop, D.R., Jimenez, J.L., 2006. Anal. Chem. 78, 8281–8289.
Diana, L.G., Mark, Z.J., 2012. Environ. Res. Lett. 7, 045901.
Drinovec, L., Močnik, G., Zotter, P., Prévôt, A.S.H., Ruckstuhl, C., Coz, E., Rupakheti, M., Sciare, J., Müller, T., Wiedensohler, A., Hansen, A.D.A., 2014. Atmos. Meas. Tech. 8, 1965–1979.
Durbin, T.D., Miller, J.W., Younglove, T., Huai, T., Cocker, K., 2007. Environ. Sci. Technol. 41, 4059–4064.
Erlandsson, L., Sandstroem-Dahl, C., Gasste, J., Lindgren, M., 2010. SAE Int. 3, 453–466.
European Commission, 2008. Off. J. Eur. Comm. L199, 1–136.
European Commission, 2009. Off. J. Eur. Comm. L140/88.
European Commission, 2013. COM 175.
Gordon, T.D., Presto, A.A., May, A.A., Nguyen, N.T., Lipsky, E.M., Donahue, N.M., Gutierrez, A., Zhang, M., Maddox, C., Rieger, P., Chattopadhyay, S., Maldonado, H., Maricq, M.M., Robinson, A.L., 2014. Atmos. Chem. Phys. 14, 4661–4678.
Gordon, T.D., Presto, A.A., Nguyen, N.T., Robertson, W.H., Na, K., Sahay, K.N., Zhang, M., Maddox, C., Rieger, P., Chattopadhyay, S., Maldonado, H., Maricq, M.M., Robinson, A.L., 2014. Atmos. Chem. Phys. 14, 4643–4659.
Graham, L.A., Belisle, S.L., Baas, C.-L., 2008. Atmos. Environ. 42, 4498–4516.
Graham, L.A., Belisle, S.L., Rieger, P., 2009. Atmos. Environ. 43, 2031–2044.
Grosjean, D., Grosjean, E., Moreira, L.F.R., 2002. Environ. Sci. Technol. 36, 1389–1395.
Heeb, N., Czerwinski, J., Zimmerli, Y., Forss, A., Hilfiker, T., Bach, C., 2010. SAE Tech. Pap. Ser. 3, 1099–1112.
Hallquist, M., Wenger, J.C., Baltensperger, U., Rudich, Y., Simpson, D., Claeys, M., Dommen, J., Donahue, N.M., George, C., Goldstein, A.H., Hamilton, J.F., Herrmann, H., Hoffmann, T., Iinuma, Y., Jang, M., Jenkin, M.E., Jimenez, J.L., Kiendler-Scharr, A., Maenhaut, W., McFiggans, G., Mentel, T.F., Monod, A., Prévôt, A.S.H., Seinfeld, J.H., Surratt, J.D., Szmigielski, R., Wildt, J., 2009. Atmos. Chem. Phys. 9, 5155–5236.
Hellebust, S., Temime-Roussel, B., Bertrand, A., Platt, S. M., Haddad, I. E., Pieber, S. M., Zardini, R., Suarez-Bertoa, A. A., Slowik, J. G., Huang, R. J., Mocnik, G., Astorga, C., Baltensperger, U., Prévôt, A. S. H., Marchand, N., 2015. (in prep).
Hildebrandt, L., Donahue, N.M., Pandis, S.N., 2009. Atmos. Chem. Phys. 9, 2973–2986.
Huai, T., Durbin, T.D., Miller, J.W., Pisano, J.T., Sauer, C.G., Rhee, S.H., Norbeck, J.M., 2003. Environ. Sci. Technol. 37, 4841–4847.
Jacobson, M.Z., 2007. Environ. Sci. Technol. 41, 4150–4157.
Jang, M., Kamens, R.M., 2001. Environ. Sci. Technol. 35, 4758–4766.
Jang, M., Czoschke, N.M., Lee, S., Kamens, R.M., 2002. Science 298, 814–817.
Jimenez, J.L., Canagaratna, M.R., Donahue, N.M., Prevot, A.S.H., Zhang, Q., Kroll, J.H., DeCarlo, P.F., Allan, J.D., Coe, H., Ng, N.L., Aiken, A.C., Docherty, K.S., Ulbrich, I.M., Grieshop, A.P., Robinson, A.L., Duplissy, J., Smith, J.D., Wilson, K.R., Lanz, V.A., Hueglin, C., Sun, Y.L., Tian, J., Laaksonen, A., Raatikainen, T., Rautiainen, J., Vaattovaara, P., Ehn, M., Kulmala, M., Tomlinson, J.M., Collins, D.R., Cubison, M.J., Dunlea, E.J., Huffman, J.A., Onasch, T.B., Alfarra, M.R., Williams, P.I., Bower, K., Kondo, Y., Schneider, J., Drewnick, F., Borrmann, S., Weimer, S., Demerjian, K., Salcedo, D., Cottrell, L., Griffin, R., Takami, A., Miyoshi, T., Hatakeyama, S., Shimono, A., Sun, J.Y., Zhang, Y.M., Dzepina, K., Kimmel, J.R., Sueper, D., Jayne, J.T., Herndon, S.C., Trimborn, A.M., Williams, L.R., Wood, E.C., Middlebrook, A.M., Kolb, C.E., Baltensperger, U., Worsnop, D.R., 2009. Science 326, 1525–1529.
Kalberer, M., Sax, M., Samburova, V., 2006. Environ. Sci. Technol. 40, 5917–5922.
Karavalakis, G., Short, D., Vu, D., Villela, M., Asa-Awuku, A., Durbin, T.D., 2014. Fuel 128, 410–421.
Kean, A.J., Littlejohn, D., Ban-Weiss, G.A., Harley, R.A., Kirchstetter, T.W., Lunden, M.M., 2009. Atmos. Environ. 43, 1565–1570.
Kroll, J.H., Seinfeld, J.H., 2008. Atmos. Environ. 42, 3593–3624.
Livingston, C., Rieger, P., Winer, A., 2009. Atmos. Environ. 43, 3326–3333.
Mathis, U., Mohr, M., Forss, A.-M., 2005. Atmos. Environ. 39, 107–117.
Millet, D.B., Guenther, A., Siegel, D.A., Nelson, N.B., Singh, H.B., de Gouw, J.A., Warneke, C., Williams, J., Eerdekens, G., Sinha, V., Karl, T., Flocke, F., Apel, E., Riemer, D.D., Palmer, P.I., Barkley, M., 2010. Atmos. Chem. Phys. 10, 3405–3425.
Millet, D.B., Apel, E., Henze, D.K., Hill, J., Marshall, J.D., Singh, H.B., Tessum, C.W., 2012. Environ. Sci. Technol. 47, 2141–2141.
Millet, D.B., Apel, E., Henze, D.K., Hill, J., Marshall, J.D., Singh, H.B., Tessum, C.W., 2012. Environ. Sci. Technol. 47, 2141–2141.
Ng, N.L., Canagaratna, M.R., Zhang, Q., Jimenez, J.L., Tian, J., Ulbrich, I.M., Kroll, J.H., Docherty, K.S., Chhabra, P.S., Bahreini, R., Murphy, S.M., Seinfeld, J.H., Hildebrandt, L., Donahue, N.M., DeCarlo, P.F., Lanz, V.A., Prévôt, A.S.H., Dinar, E., Rudich, Y., Worsnop, D.R., 2010. Atmos. Chem. Phys. 10, 4625–4641.
Nguyen, H.T.-H., Takenaka, N., Bandow, H., Maeda, Y., de Oliva, S.T., Botelho, M. M. f., Tavares, T.M., 2001. Atmos. Environ. 35, 3075–3083.
Orlando, J., Brasseur, G., Tyndall, G., 1999. Atmospheric Chemistry and Global Change. Oxford University Press.
Phuleria, H.C., Geller, M.D., Fine, P.M., Sioutas, C., 2006. Environ. Sci. Technol. 40, 4109–4118.
Pitts, J.N., Finlayson-Pitts, B.J., 2000. Chemistry of the Upper and Lower Atmosphere: Theory, Experiments, and Applications. Academic Press, New York.
Platt, S.M., El Haddad, I., Zardini, A.A., Clairotte, M., Astorga, C., Wolf, R., Slowik, J.G., Temime-Roussel, B., Marchand, N., Ježek, I., Drinovec, L., Močnik, G., Möhler, O., Richter, R., Barmet, P., Bianchi, F., Baltensperger, U., Prévôt, A.S.H., 2013. Atmos. Chem. Phys. 13, 9141–9158.
Platt, S.M., Haddad, I.E., Pieber, S.M., Huang, R.J., Zardini, A.A., Clairotte, M., Suarez-Bertoa, R., Barmet, P., Pfaffenberger, L., Wolf, R., Slowik, J.G., Fuller, S.J., Kalberer, M., Chirico, R., Dommen, J., Astorga, C., Zimmermann, R., Marchand, N., Hellebust, S., Temime-Roussel, B., Baltensperger, U., Prévôt, A.S.H., 2014. Nat. Commun. 5.
Pope, I.C., Burnett, R.T., Thun, M.J., et al., 2002. J. Am. Med. Assoc. 287, 1132–1141.
Prinn, R.G., Huang, J., Weiss, R.F., Cunnold, D.M., Fraser, P.J., Simmonds, P.G., McCulloch, A., Harth, C., Salameh, P., O'Doherty, S., Wang, R.H.J., Porter, L., Miller, B.R., 2001. Science 292, 1882–1888.
Ramaswamy, V., Forster, P., Artaxo, P., Berntsen, T., Betts, R., Fahey, D.W., Haywood, J., Lean, J., Lowe, D.C., Myhre, G., Nganga, J., Prinn, R., Raga, G., Schulz, M., Van Dorland, R., 2007. Changes in atmospheric constituents and in radiative forcing. In: Climate Change 2007: the Physical Science Basis. United Kingdom and New York, NY, USA.
Reinhardt, A., Emmenegger, C., Gerrits, B., Panse, C., Dommen, J., Baltensperger, U., Zenobi, R., Kalberer, M., 2007. Anal. Chem. 79, 4074–4082.
Saleh, R., Robinson, E.S., Tkacik, D.S., Ahern, A.T., Liu, S., Aiken, A.C., Sullivan, R.C., Presto, A.A., Dubey, M.K., Yokelson, R.J., Donahue, N.M., Robinson, A.L., 2014. Nat. Geosci. 7, 647–650.
Suarez-Bertoa, R., Zardini, A.A., Astorga, C., 2014. Atmos. Environ. 97, 43–53.
Taira, M., Kanda, Y., 1990. Anal. Chem. 62, 630–633.
Tan, Y., Carlton, A.G., Seitzinger, S.P., Turpin, B.J., 2010. Atmos. Environ. 44, 5218–5226.
The Council of the European Communities, 1970. Off. J. Eur. Communities 1–22.
The European Parliament and The Council of the European Union, 2002. Off. J. Eur. Communities L67.
Wallner, T., 2011. J. Eng. Gas. Turb. Power 133, 082801–082801.
Westerholm R., 2008. www.biofuels-platform.ch/en/media/download.php?get=130.
Whittington, B.I., Jiang, C.J., Trimm, D.L., 1995. Catal. Today. 26, 41–45.
Williams, L.R., Gonzalez, L.A., Peck, J., Trimborn, D., McInnis, J., Farrar, M.R., Moore, K.D., Jayne, J.T., Robinson, W.A., Lewis, D.K., Onasch, T.B., Canagaratna, M.R., Trimborn, A., Timko, M.T., Magoon, G., Deng, R., Tang, D., de la Rosa Blanco, E., Prévôt, A.S.H., Smith, K.A., Worsnop, D.R., 2013. Atmos. Meas. Tech. 6, 3271–3280.
Zardini, A.A., Platt, S.M., Clairotte, M., El Haddad, I., Temime-Roussel, B., Marchand, N., Ježek, I., Drinovec, L., Močnik, G., Slowik, J.G., Manfredi, U., Prévôt, A.S.H., Baltensperger, U., Astorga, C., 2014. Atmos. Environ. 94, 307–315.